Atomic insights into hydrodesulfurization

Prabhu, M.K.

Chapter 2

Experimental Methods

2.0 The ReactorSTM setup

All the experiments presented in this thesis were carried out in the ReactorSTM ultra-high vacuum (UHV) setup shown in Figure 1.[1] The ReactorSTM has three stainless steel chambers which house the high-pressure scanning tunneling microscope (STM), a combined low-energy electron diffraction (LEED) - Auger electron spectroscopy (AES) apparatus, an X-ray photoelectron spectroscopy (XPS) system and the sample preparation facilities.

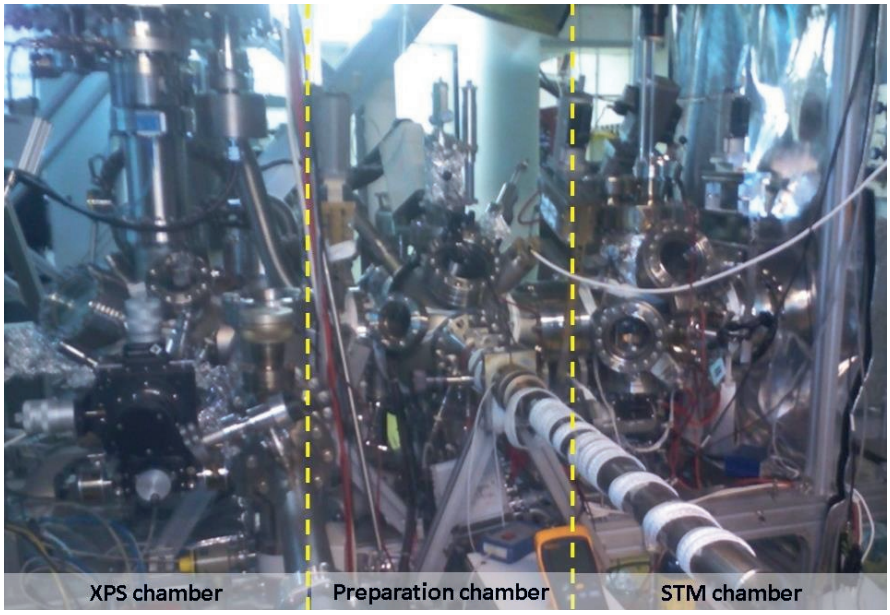

Figure 1: A photograph of the ReactorSTM setup.

The high-pressure STM is housed in the first chamber, the sample preparation and LEED/AES are housed in the second chamber called the "preparation chamber" and the XPS is in the third chamber. A transfer arm is used to move the sample between the chambers without air exposure. All the three chambers are independently pumped by ion pumps and are maintained at UHV conditions. The preparation chamber has a commercial sputtering gun, an e-beam evaporator and leak valves for dosing gases such as Ar, H_2, O_2, and H_2S. For reaching high local pressures of oxygen, the respective leak valve is attached to a doser which can be extended to reach very close to the surface of the sample. The sample heating is carried out using radiation and e-beam heating via a filament of thoriated-tungsten placed at the back of the sample inside the sample holder. Furthermore, there is also a load-lock system for transferring the samples from air into the UHV without breaking the vacuum.

2.0.1 Scanning tunneling microscope (STM)

Figure 2 shows the schematic with the essential components of a scanning tunneling microscope. An atomically sharp tip made of a wire of tungsten or Pt-Ir alloy, which is used as the probe, is attached to a piezoelectric scanner. The piezo electric scanner has orthogonal transducers along the X, Y, and Z directions each with a separate electronic connection. Application of a suitable voltage at each of these connections can be used to actuate the piezo, and hence the tip, in the three Cartesian directions. With the help of a coarse motor and by the application of a voltage along the Z direction, the atomically sharp tip is brought within a few angstroms of the sample of interest. Thereafter, a voltage is applied between the tip and sample to establish a tunneling junction. By applying a saw-tooth voltage input at X and a ramp input at Y, the tip can be moved in a raster manner across the surface. A preamplifier is used to boost the tunneling current signal which is then sent to a feedback system. The feedback system calculates the error in the tunneling current with respect to a user-decided set point. Using this error, the feedback acts on the Z voltage to reduce the error and maintain the tunneling current. Thus, by recording the tunneling current in a raster manner, a spatial map of the local density of states (LDOS) can be generated. This map is plotted on the computer screen as the STM image. The entire STM assembly has to be vibrationally isolated from the surroundings as electron tunneling is a very sensitive phenomenon. Such a vibrational isolation is achieved by suspending the rigid STM assembly on an eddy-current damping system. STM is a very robust technique than can be operated from near absolute zero to several hundred kelvin temperatures, in vacuum and high-pressure of gases, in liquids and electrochemical environments as long as there is a conducting sample to study. A detailed description of an STM can be found elsewhere.[2]

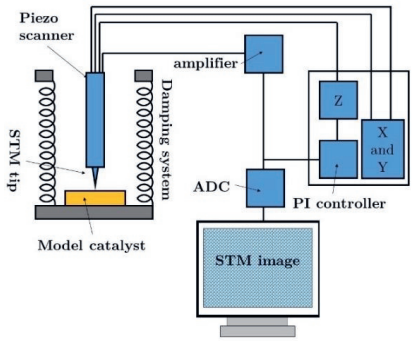

Figure 2. Schematic of a scanning tunneling microscope

The tunneling current I is a function of the applied voltage V, location z, local density of states ρ, mass of electron m, work function of the material φ and Planck constant h. This is represented by the equation:

$$I \propto V \rho e^{\frac{-4\pi z\sqrt{2m\varphi}}{h}} \tag{2.1}$$

Near the Fermi level, this equation can be written as:

$$I \propto V \rho_s e^{-1.025 z\sqrt{\varphi}} \tag{2.2}$$

Thus, there is a direct proportionality between I and applied voltage V. I exponentially decays ($\sim e^{-2.292}$ for $\varphi = 5$ eV) with the tip-sample distance z. Therefore, small changes in the tip-sample distance result in large variations in the tunneling current. The feedback system makes use of this property to apply the corrections in the Z voltage to maintain the tunneling current. As is evident from Equation 2.2, a conducting surface is necessary to have a finite ρ_s and a non-zero I.[2,3]

2.0.2 High-pressure STM

Heterogeneous catalysis is driven by surface reactions and therefore, understanding the surface structure of the catalyst is necessary for establishing the structure-activity relationships. A large number of catalytic processes use a catalysts that involve metal or metal sulfide nanoparticles supported on a metal oxide surface. Being one of the few techniques which are sensitive to the surface at the atomic level and one that does not impose limitations at the fundamental level when bridging the pressure gap, STM is an ideal technique to study model catalysts at industrially relevant conditions and resolve many of the unsolved problems of catalysis.[1,4]

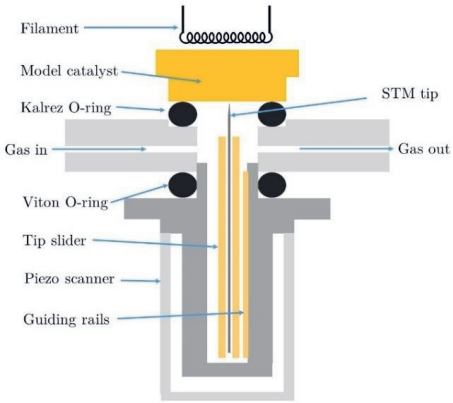

Figure 3. Schematic of the high-pressure STM for studying model catalysts at industrially relevant conditions based on Herbschleb et al.[1]

Figure 3 shows the schematic cross section of the high-pressure STM used in the studies presented in this thesis. The high-pressure STM assembly consists of a combination of the STM itself, the reactor volume, and the sample holder. The construction of the STM is such that the volume of the reactor formed by pressing the sample holder against the STM is 50 µL. The reactor is sealed vacuum tight from the rest of the assembly and the UHV components by two chemically inert elastomer O-rings as shown in Figure 3. The lower seal in Figure 3 is made up of Viton while the upper seal between the

sample and the STM is made up of Kalrez. The use of these O-rings limits the operating temperature to 600 K. The hat-shaped sample of interest is electrically isolated from the sample holder and has a filament mounted at its rear for radiative heating. K-type thermocouples welded on to the sample allow for direct temperature measurement. A set of bellows are used to press the sample, the Kalrez O-ring, and the STM together to establish a closed reactor cell. Capillary-size channels are present in the reactor volume to allow for the flow of gases. The channels are directly connected to a dedicated gas cabinet and a quadrupole mass spectrometer to control and monitor the flow of gases. A total operating pressure of up to 6 bar is possible. For establishing the tunneling junction, a single piezo tube is used for both the coarse Z approach and the raster scanning motion. The STM tip is placed within a gold-coated stainless-steel holder which is actuated by an SmCo magnet against a pair of gold-coated rails to allow for optimum stick-slip behavior and chemical inertness of these metallic parts. The magnet is chosen such that the force generated by the magnet overcomes the static friction between the tip holder and the guiding rails. A set of video-rate scanning electronics allows for the acquisition of the STM images at up to ~1 image/second with a resolution of 256 x 256 square pixels. Typically, operando STM images are acquired at 512 x 512 square pixel resolution with an acquisition time of 10-20 seconds.[1,5,6]

A typical experiment with the high-pressure STM starts with the preparation of the model catalyst in the preparation chamber according to the desired recipe. Meanwhile, the gas dosing system is baked out at ~423 K for several hours under the flow of Ar gas to remove any residual gasses and impurities. The prepared model catalyst is then loaded into the STM by the means of a transfer arm. At this stage, the Kalrez O-ring is placed on the reactor with the help of a wobble stick. The bellows of the reactor and the damping system are then actuated to close the gap between the reactor and the model catalyst. This ensures that the Kalrez O-ring makes a vacuum-tight contact with the sample and the reactor body as is shown in Figure 3. The gas dosing system is designed such that the closed reactor volume, thus formed, may either be maintained at UHV or be pressurized with the reaction gasses without breaking the UHV outside the reactor volume. In this manner, only the model catalyst, the STM tip, the slider and the Kalrez O-ring are exposed to the reaction gasses. In order to reach the desired operating conditions, the reactor is initially pressurized with the reaction gasses to up to 0.1 bar. Thereafter, the temperature of the sample is increased at a rate of at most 10 K/min to the desired value. A slow heating rate is used in order to ensure that the thermal gradient within the Kalrez O-ring is gradual so that failure of the O-ring may be avoided. Once the operating temperature is reached, the system is allowed to stabilize for at least 60 minutes. Thereafter, the reactor is pressurized at the rate of 0.01 bar per minute to the desired operating pressure with the reaction gasses. The system is then allowed to stabilize for at least 60 minutes before commencing the scan. During the time that is taken to go from UHV condition to the industrial reaction conditions, changes that occur on the model catalyst cannot be observed as the imaging is commenced only after several hours, when the system is thoroughly stabilized. However, the long term effects of the reaction gasses on the catalyst morphologies can be observed with the high-pressure STM. Furthermore, after the system is stabilized, the processes which occur on the time scale of a few seconds or more may also be imaged with the high-pressure STM if sufficiently fast image acquisition rates are used.

2.1 X-ray photoelectron spectroscopy

While the STM is excellent for atomic resolution of the surface of a model catalyst, it does not provide any direct chemical information and hence, should be supplemented by a technique which is surface sensitive and also provides chemical information. XPS works by the principle of the photoelectric effect and its probing depth is determined by the mean free path of the electrons in the sample. This allows for high surface sensitivity. There are four main processes which occur during XPS characterization: Excitation of the sample with X-ray photons, ejection of core-level electrons from the atoms present in the sample, interaction of these electrons with the atoms in the sample all the way to the surface leading to elastic and inelastic scattering, electrons leaving the sample at the surface and traversing through the vacuum to reach the detector. The schematic in Figure 4 describes the basic principle of operation of an XPS.[7] For a photon energy hν where ν is the frequency and h is the Plank constant, the kinetic energy of the ejected electron is given by:

$$E_{kin} = h\nu - E_{bin} - \varphi_a \qquad (2.3),$$

where φ_a is the work function of the analyzer and E_{bin} is the binding energy of the core electron. The photoelectron's kinetic energy depends on the interaction of the atoms with their nearest neighbors and hence, by measuring E_{kin}, we can obtain direct chemical information of the model catalyst.

Electrons generated by a tungsten filament in vacuum are accelerated on to an anode by applying a high voltage. The anode is typically made of Al or Mg. The incident high-energy electron beam generates core-level holes in the anode material. The relaxation of the electrons from the higher levels into the core hole leads to the emission of X-ray photons. The characteristics of these photons are described by the K-shell emission lines of the anode. Using a set of X-ray optics in a monochromator, the K_α emission line alone is selected and the other emission lines and Bremsstrahlung are filtered out.[8]

When the X-ray photons strike the model catalyst, core-level electrons of the atoms, which are excited by the X-rays, are ejected out. These ejected electrons interact strongly with the atoms they encounter along their path. The mean free path of electrons in solids is typically only about 7-10 atomic layers for electron energies varying from 100-1000 eV which are typically encountered in the XPS analysis.[9] Therefore, only those photoelectrons within the first 7-10 atomic layers below the surface of the model catalyst manage to reach the surface and escape into the vacuum.

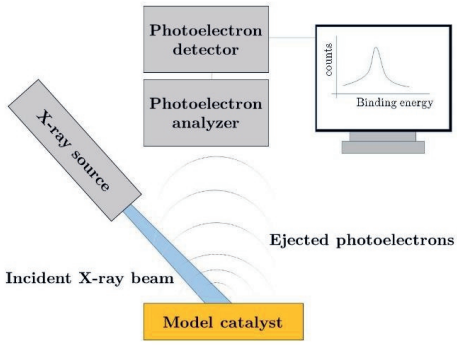

Figure 4. Schematic of the X-ray photoelectron spectroscopy apparatus

An electron analyzer captures these electrons and sorts them according to their kinetic energies. The analyzer typically performs the role of a band-pass filter for analyzing the incoming photoelectrons from the sample. The analyzer collects these photoelectrons and measures their intensity as a function of kinetic energy. Using Equation 2.3, a plot of binding energy vs intensity is generated. Analysis of the peaks in this plot gives information of the chemical state of the sample.[8]

2.2 Low-energy electron diffraction (LEED)

LEED is a powerful surface-sensitive technique for revealing the atomic structure of surfaces. Historically, LEED has been used to resolve the structure of a variety of metal and semiconductor surfaces and is an essential tool for structure determination in surface science.[10–12] LEED is particularly useful for this as it is sensitive to the actual positions of the atoms. In this study, LEED has been used to resolve the structure of 2D CoS_2 in Chapter 3.

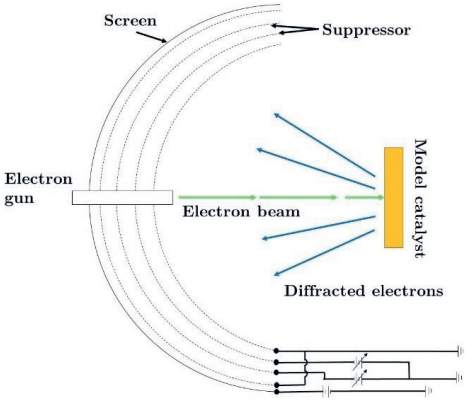

Figure 5. Schematic of the LEED apparatus based on Van Hove et al.[12]

The schematic of a typical LEED apparatus is shown in Figure 5. This apparatus consists of a 4-grid retarding field analyzer (RFA). The grids are hemispherical and concentric with the fluorescent screen on which the diffraction pattern is displayed. The electron gun is in the center through which a beam of electrons is accelerated and is incident on the sample. The electrons undergo diffraction by interacting with the surface atomic structure. The diffracted beam reflects back at the 4-grid RFA. The first grid is electrically grounded in order to maintain the region between the sample and the first grid field free. Negative potentials are applied to the second and the third grid to select diffracted electrons of a narrow energy range to be allowed to reach the fluorescent screen. The fourth grid is also grounded to ensure that the electrical fields from the fluorescent screen do not penetrate the region between the first and the fourth grid and disturb the band-filtering process of the second and the third grids. A large positive voltage (6-8 kV) is applied to the fluorescent screen to accelerate the filtered electrons and strike them against the screen and render the diffraction spots visible. By analyzing the diffraction pattern, the reciprocal-space lattice of the surface structure can be determined. From the reciprocal-space lattice, the real-space periodicity of the surface can be calculated. A detailed description of the LEED apparatus can be found elsewhere.[10–12]

2.3 References

(1) Herbschleb, C. T.; Van Der Tuijn, P. C.; Roobol, S. B.; Navarro, V.; Bakker, J. W.; Liu, Q.; Stoltz, D.; Cañas-Ventura, M. E.; Verdoes, G.; Van Spronsen, M. A.; Bergman, M.; Crama, L.; Taminiau, I.; Ofitserov, A.; Van Baarle, G. J. C.; Frenken, J. W. M. The ReactorSTM: Atomically Resolved Scanning Tunneling Microscopy under High-Pressure, High-Temperature Catalytic Reaction Conditions. *Rev. Sci. Instrum.* 2014, *85* (8). https://doi.org/10.1063/1.4891811.

(2) Chen, C. J. *Introduction to Scanning Tunneling Microscopy: Second Edition*; 2007; Vol. 9780199211. https://doi.org/10.1093/acprof:oso/9780199211500.001.0001.

(3) Kuk, Y.; Silverman, P. J. Scanning Tunneling Microscope Instrumentation. *Review of Scientific Instruments*. 1989, pp 165–180. https://doi.org/10.1063/1.1140457.

(4) Laegsgaard, E.; Österlund, L.; Thostrup, P.; Rasmussen, P. B.; Stensgaard, I.; Besenbacher, F. A High-Pressure Scanning Tunneling Microscope. *Rev. Sci. Instrum.* 2001, *72* (9), 3537–3542. https://doi.org/10.1063/1.1389497.

(5) Rost, M. J.; Crama, L.; Schakel, P.; Van Tol, E.; Van Velzen-Williams, G. B. E. M.; Overgauw, C. F.; Ter Horst, H.; Dekker, H.; Okhuijsen, B.; Seynen, M.; Vijftigschild, A.; Han, P.; Katan, A. J.; Schoots, K.; Schumm, R.; Van Loo, W.; Oosterkamp, T. H.; Frenken, J. W. M. Scanning Probe Microscopes Go Video Rate and Beyond. *Rev. Sci. Instrum.* 2005, *76* (5). https://doi.org/10.1063/1.1915288.

(6) Rost, M. J.; van Baarle, G. J. C.; Katan, A. J.; van Spengen, W. M.; Schakel, P.; van Loo, W. A.; Oosterkamp, T. H.; Frenken, J. W. M. Video-Rate Scanning Probe Control Challenges: Setting the Stage for a Microscopy Revolution. *Asian J. Control* 2009, *11* (2), 110–129. https://doi.org/10.1002/asjc.88.

(7) Pomeransky, A. A.; Khriplovich, I. B. *Equations of Motion of Spinning Relativistic Particle in External Fields*; 1999; Vol. 14. https://doi.org/10.1080/01422419908228843.

(8) Rivière, J. C. Surface Analysis. In *Handbook of Analytical Techniques*; 2008; Vol. 2–2, pp 851–949. https://doi.org/10.1002/9783527618323.ch27.

(9) Gall, D. Electron Mean Free Path in Elemental Metals. *J. Appl. Phys.* 2016, *119* (8). https://doi.org/10.1063/1.4942216.

(10) Held, G. Low-Energy Electron Diffraction (LEED). In *Surface and Thin Film Analysis: A Compendium of Principles, Instrumentation, and Applications, Second Edition*; 2011; pp 93–109. https://doi.org/10.1002/9783527636921.ch5.

(11) Jona, F.; Strozier, J. A.; Yang, W. S. Low-Energy Electron Diffraction for Surface Structure Analysis. *Reports Prog. Phys.* 1982, *45* (5), 527–585. https://doi.org/10.1088/0034-4885/45/5/002.

(12) VanHove, Michel A., Weinberg, William Henry, Chan, C.-M. *Low-Energy Electron Diffraction*; Ertl, G., Ed.; Springer-Verlag, 1986.